Chemical and Process Engineering: New Frontiers, 2023, 44(3), e21
DOI: 10.24425/cpe.2023.146723

Peroxymonosulfate-assisted photocatalytic degradation of artificial sweeteners in water

Jakub Smoliński[1], Agnieszka Fiszka Borzyszkowska[1], Paweł Kubica[2], Anna Zielińska-Jurek[1*]

[1] Gdańsk University of Technology, Faculty of Chemistry, Department of Process Engineering and Chemical Technology, Narutowicza 11/12, 80-233 Gdańsk, Poland
[2] Gdańsk University of Technology, Faculty of Chemistry, Department of Analytical Chemistry, Narutowicza 11/12, 80-233 Gdańsk, Poland

*** Corresponding author:**
e-mail:
annjurek@pg.edu.pl

Presented at 24th Polish Conference of Chemical and Process Engineering, 13–16 June 2023, Szczecin, Poland.

Article info:
Received: 5 May 2023
Revised: 26 June 2023
Accepted: 14 July 2023

Abstract
In the present study, peroxymonosulfate (PMS) activation was proposed for efficient photocatalytic degradation of aspartame, acesulfame, saccharin, and cyclamate – artificial sweeteners frequently present in wastewaters and surface waters worldwide. TiO_2 nanosheets with exposed {0 0 1} facets were synthesised using the fluorine-free lyophilisation technique as a green concept for the synthesis and used for the photodegradation of selected sweeteners not susceptible to biodegradation. The synergetic effect of photocatalysis with the sulfate radical-based process was for the first time investigated. It was found that the studied artificial sweeteners were practically not susceptible to photolysis within 60 minutes of irradiation. In the presence of 2D titanium (IV) oxide, the artificial sweeteners were degraded entirely in less than 30 min, whereas the addition of peroxymonosulfate resulted in complete degradation after 10–15 minutes of the process.

Keywords
artificial sweeteners, acesulfame degradation, 2D TiO_2, photocatalysis, PMS-assisted photodegradation

1. INTRODUCTION

Progressive pollution of the aquatic environment related to the presence of emerging contaminants results from their resistance to conventional wastewater treatment processes. Artificial sweeteners include substances from several different chemical classes interacting with taste receptors, which are widely used as sugar substitutes and added to food, beverages, pharmaceuticals, and personal care products (Praveena et al., 2019). Although the measured concentrations of the most persistent artificial sweeteners range to microgram per litre levels in surface waters, chronic exposure to these compounds can induce long-term environmental and health effects (Cong et al., 2013; Erbaş et al., 2018; Naik et al., 2021). Therefore, the highly water soluble and persistent to biodegradation artificial sweeteners have been recognised as emerging contaminants. Among the variety of artificial sweeteners commonly used, primary acesulfame (ACE), cyclamate (CYC), saccharin (SACH), and sucralose (SUC) have been detected in wastewater effluents (Sang et al., 2014).

Furthermore, especially acesulfame and sucralose are found in the aquatic environment at the highest median concentrations of about hundreds of ng·dm^{-3} than most pharmaceuticals, personal care products, and other wastewater-specific anthropogenic organic chemicals (Zhong et al., 2021) and therefore identified as emerging contaminants in water. Acesulfame, 150 times sweeter than sucrose, is a cyclic sulfonamide derivative that is not metabolised and excreted by humans in an unchanged form. Therefore, acesulfame is proposed as a tracer of anthropogenic activity (Sang et al., 2014; Toth et al., 2012). Next to acesulfame, aspartame (ASP) and cyclamate (CYC) have been reported as the most persistent sweeteners. Aspartame, a high-intensity sweetener, is produced in the amount of about 16,000 tons annually in North America for worldwide consumption (Kokotou et al., 2012). Considering incomplete metabolisation, this sweetener is excreted primarily unchanged from the human body, and as a result of decomposition into phenylalanine and aspartic acid, it cannot be consumed by people suffering from phenylketonuria. In acidic aqueous solutions at a pH of 4–5, aspartame is a stable compound with a half-life of about 300 days (Jia et al., 2014). Aspartame is often mixed with another sweetener, such as cyclamate, due to its bitter aftertaste. In 1970 Food and Drug Administration in US prohibited the use of cyclamate (E-952) because of the detection of bladder tumors in rodents (Oser et al., 1975). However, cyclamate is still approved in over 50 countries (Basson et al., 2021). Furthermore, some intestinal bacteria can metabolise cyclamate to toxic cyclohexylamine (Renwick et al., 2004).

In this regard, in the present study, a combination of the photocatalytic process with peroxymonosulfate (PMS) activation was proposed for efficient photodegradation of artificial sweeteners frequently present in wastewaters and surface waters worldwide.

The advanced oxidation processes (AOP), based on the in-situ generation of the strongest oxidants – hydroxyl radicals

and sulfate radicals, have been recognised as a promising approach for wastewater treatment from residues of recalcitrant and emerging organic contaminants. Perkola et al. (2016) studied the direct and indirect photochemical decomposition of acesulfame, saccharin, cyclamic acid and sucralose in environmentally relevant dilute aqueous solutions. It was observed that acesulfame might be susceptible to photodegradation in surface waters, while saccharin, cyclamic acid and sucralose degrade very slowly, even under energetic UV light irradiation (Perkola et al., 2016). Furthermore, photocatalysis has been proposed as a promising method for the degradation of persistent artificial sweeteners acesulfame and saccharin under UV-A irradiation in the presence of commercial TiO_2 (Zelinski et al., 2018).

Simultaneously, the sulfate radical-based ($SO_4^{\bullet -}$) process has recently received growing attention as a desirable method for degrading recalcitrant pollutants (Wacławek et al., 2017). In comparison to the hydroxyl radicals, predominately generated in-situ during most of the AOP processes, the sulfate radical-based AOPs are characterised by similar or even higher redox potential ($E^0 = 2.6 - 3.1 V_{NHE}$ vs. 1.8–2.7 V_{NHE} for $^{\bullet}OH$) and longer half-life (30–40 μs) than the $^{\bullet}OH$ (less than 1 μs) radicals (Wang et al., 2019a). SR-AOPs are more suitable for organic pollutant degradation regardless of operating conditions, as $SO_4^{\bullet -}$ can react efficiently in a wide pH range from 2 to 8 (Yang et al., 2021). For example, sucralose, one of the newest artificial sweeteners, was almost completely degraded and mineralised using UV/PMS system within 60 min of irradiation under UV light (Xu et al., 2017). Wang et al. (2019b) studied the degradation of acesulfame under UV-LED controlled illumination in the presence of titanium(IV) oxide (TiO_2), zinc(II) oxide (ZnO) as photocatalysts, UV/H_2O_2 process, peroxomonosulfate-assisted (PMS, HSO_5^-) and peroxodisulfate-assisted (PDS, $S_2O_8^{2-}$) SR-AOP processes (Wang et al., 2019b). However, to the best of our knowledge, there is no study on the peroxymonosulfate-assisted photocatalytic degradation of artificial sweeteners. Therefore, in the present work, we have proposed the selected light-induced processes for efficient photocatalytic degradation of aspartame, potassium acesulfame, sodium saccharin, and sodium cyclamate.

In the present study, TiO_2 nanosheets with exposed {0 0 1} facets were synthesised using the fluorine-free lyophilisation technique as a green concept for the synthesis and used for the photodegradation of artificial sweeteners. The ultrathin 2D TiO_2 nanosheets were used as a promising photocatalytic material that allows to minimise the diffusion distance, whose photoinduced electron-hole pairs must overcome before reaching the solid-water interface, which may result in reduced photoinduced charge carrier recombination during transport. Moreover, TiO_2 nanosheets provide many active sites for photocatalytic reactions, allowing the facile adhesion of organic molecules and improving functionality (Malinowska et al., 2023). The comprehensive analysis of the selected artificial sweeteners' photodegradation by photolysis, photocatalysis in the presence of 2D TiO_2, PMS/UV system and the enhanced PMS/TiO_2/UV were studied in detail. Furthermore, the synergetic effect of photocatalysis with the sulfate radical-based process was investigated.

2. MATERIALS AND METHODS

Artificial sweeteners: aspartame ($C_{14}H_{18}N_2O_5$), potassium acesulfame ($C_4H_4KNO_4S$), sodium saccharin ($C_7H_4NNaO_3S$) and sodium cyclamate ($C_6H_{12}NNaO_3S$) and peroxymonosulfate (PMS) were obtained from Sigma-Aldrich, Germany. Titanium(IV) oxysulphate ($TiOSO_4 \cdot xH_2O$) was provided by Sigma Aldrich and used for titanium(IV) oxide synthesis. Hydrogen peroxide solution (H_2O_2, 30%), ammonia water (NH_3, 25%), acetic acid, formic acid, acetone and methanol were provided by POCH, Poland. Acetonitrile (HPLC grade) was purchased from Supelco, and phosphoric acid (HPLC grade, 85%) from Fischer Chemical in Poland.

2.1. Preparation of 2D anatase nanosheets

In order to obtain TiO_2 nanosheets, 10 g of $TiOSO_4 \cdot xH_2O$ was added to 300 cm^3 of deionised water at 40 °C. The suspension was stirred and thermostated at the set temperature for an hour to obtain a clear, colourless solution. Then, the solution was cooled to 5 °C using an ice bath with a constant stirring, followed by the dropwise addition of ammonia water using a Pasteur pipette to set the pH of 9 and significantly increase the viscosity. After 30 minutes of stirring, the precipitate was centrifuged and washed with deionised water. The steps were repeated 5 times. The precipitate was dispersed in 300 cm^3 of deionised water, and 20 cm^3 of H_2O_2 was added with stirring. After 5 minutes – the solution turned orange. Another 20 cm^3 H_2O_2 was added, and after the next 5 minutes additional portion of H_2O_2. After each addition of the H_2O_2 solution, the pH was controlled – after adding 3 portions, the pH was about 3. The solution was aged for 48 h at 3 °C to form a yellow gel that was further lyophilised at –84 °C and a pressure of 0.6 Pa. The obtained powder was calcined with a temperature gradient of 1 °C/min at 700 °C for 1h with the formation of TiO_2 nanosheets.

2.2. Characterisation of obtained TiO_2 nanosheets

The phase composition and structure of the samples were determined using the powder X-ray diffractometer (XRD) (Cu Kα, Rigaku MiniFlex 600 X-Ray diffractometer). Analyses were performed using a HighScorePlus software package (PANalytical, 2006). Data alignment was based on the pseudo-Voigt function and the ICDD database. Data were collected in the 2θ range of 5–80 °, and scan steps were fixed at 1 °·min^{-1} and 0.01 °, respectively. The morphology of the prepared photocatalyst was determined using SEM (PhenomPro G6) microscope. Brunauer–Emmett–Teller (BET) surface area analysis was performed using

a Micromeritics Gemini V instrument. The analysed samples with a mass of 0.3 g were degassed for 2 hours at 200 °C in the Micromeritics FlowPrep 060 apparatus. Adsorption took place at the boiling point of liquid nitrogen –77K. Helium was used as the carrier gas in the system. The optical properties of the photocatalyst were determined using a DR/UV-vis spectrophotometer (Thermo Fisher Scientific Evolution 220, Waltham, MA, USA) in the range of 200–800 nm, which corresponds to the photon energy of electromagnetic radiation of 6.2–1.55 eV. Barium sulfate was used as a reference material. Then, the band gap for each sample was determined based on the obtained spectra transformed into the Kubelka–Munk function and the Tauc transformation. Electrochemical impedance spectroscopy (EIS) and Mott–Schottky measurements of the photocatalyst were performed using an Autolab PGSTAT204 potentiostat/galvanostat equipped with a FRA32M module. A three-electrode cell provided by DropSens DRP 110 was used in this study, consisting of a carbon working electrode (WE) with an immobilised photocatalyst on the surface, a carbon counter electrode (CE), and a silver reference electrode (RE). An electrolyte solution was 1 M Na_2SO_4. EIS was performed under dark conditions with frequencies in the range of 1–20 000 Hz and a sinusoidal wave of 5 mV. The transient photocurrent measurement was performed with the on–off light-emitting diode (LEDs) with a near-ultraviolet (390 nm) light source at a constant potential of 0 V.

2.3. Degradation of artificial sweeteners using light-assisted processes

The light-assisted degradation processes of sweeteners were performed in a system consisting of a cylindrical reactor with a capacity of 15 cm^3, thermostated at 25 °C, magnetic stirring, and a UV medium-pressure mercury lamp (Heraeus, 150 W) as an irradiation source. The following processes were carried out for each sweetener: photolytic – UV, photolytic with PMS – UV/PMS, photocatalytic in the presence of 2D TiO_2 – UV/TiO_2 and the process in the presence of a photocatalyst and PMS – UV/TiO_2/PMS. The concentration of sweeteners in aqueous solutions was 20 mg·dm^{-3}, the photocatalyst dose was 0.5 g·dm^{-3}, while the addition of PMS was 2 mM. In the case of photocatalytic processes using 2D TiO_2, the photocatalyst suspension was stirred in the dark for 30 minutes to establish the adsorption-desorption equilibrium. Irradiation was then carried out for 60 minutes. Samples for the study of the kinetics of degradation of sweeteners in the processes mentioned above were taken after 30 minutes of the dark process and then after 5, 10, 15, 30 and 60 minutes of irradiation. For samples from processes involving PMS, the reaction was inhibited by adding methanol.

Samples taken during irradiation of sweeteners were analysed with LCMS-8060 (Shimadzu, Japan) consisting of two high-performance pumps (LC-30AD), autosampler (SIL-30AC), oven as column compartment (CTO-20AC) and valve switching (FCV-2). The mass spectrometer was equipped with an electrospray ionisation source (ESI) working with regard to the analyte in the positive and negative modes in multiple reaction monitoring (MRM). The separation of analytes was done with the use of column Zorbax XDB-C8 (150 × 4.6 mm, 3 μm). The mobile phase consisted of water with 0.05% of formic acid (FA) serving as component A and acetonitrile (ACN) with 0.05% of FA serving as component B. The flow rate was kept at 1.2 cm^3/min, while the gradient program was as follows: from 0 to 4 min, 5% of B was increased to 40% and kept for 1 minute. After that, the column was stabilised for 6 minutes at 5% of B. The injection volume into the column was 0.002 $cm^{3,}$ while the temperature of the column was maintained at 40 °C. The ion source parameters were as follows: interface temperature was 300 °C, desolvation line temperature was 250 °C and heat block temperature was 400 °C, nebulising gas, heating gas, and drying gas flow were 3, 10 and 10 dm^3/min, respectively. The parameters of the analyte for MRM transitions are presented in Table 1. Data from the mass spectrometer was gathered from 2 to 5 min with the use of LabSolution software. All calculations and data handling of the calibration curves determination was done with this software as well.

3. RESULTS AND DISCUSSION

3.1. Characteristics of the obtained photocatalyst

The morphology of the obtained TiO_2 was examined using SEM microscopy analysis. As presented in Figure 1a, TiO_2 nanosheets were successfully obtained with the lyophilisation

Table 1. Parameters of the monitored ion transitions for four analytes.

Compound	Molecular formula	Pseudomolecular ions [m/z]	Fragment ions [m/z]	Collision energy [V]
Aspartame	$C_{14}H_{18}N_2O_5$	294.90	$[M+H^+]$ **120.10** 180.10	25 14
Acesulfame-K	$C_4H_4KNO_4S$	161.80	$[M-H^-]$ **82.10** 78.00	16 29
Cyclamate-Na	$C_6H_{12}NNaO_3S$	177.90	$[M-H^-]$ **79.90***	27
Saccharine-Na	$C_7H_4NNaO_3S$	181.80	$[M-H^-]$ **105.95** 41.95	20 28

Bold – transitions used for quantitative analysis; * – only one transition could be observed

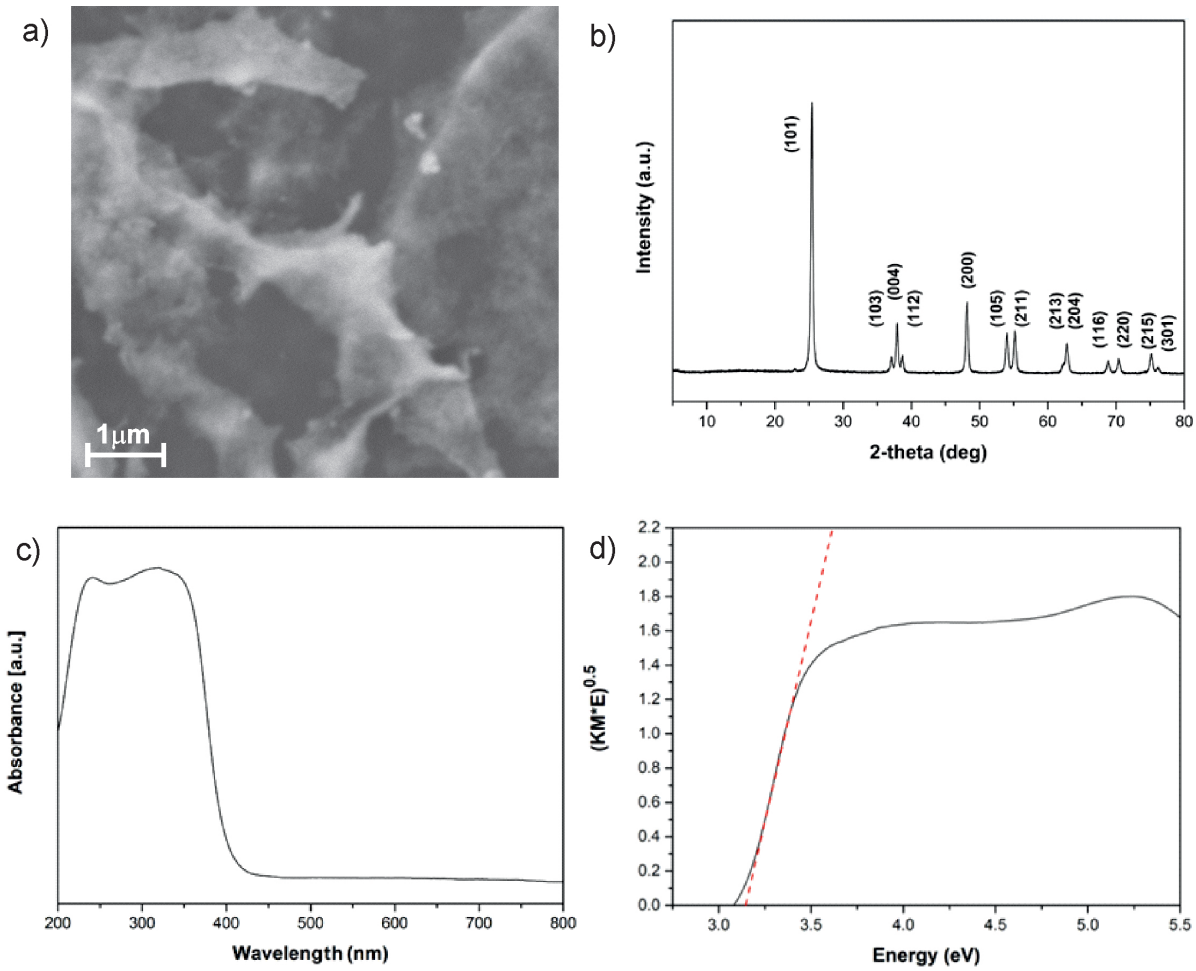

Figure 1. SEM image of 2D TiO_2 photocatalyst (a), XRD pattern for 2D TiO_2 (b), DRS UV-Vis plot of 2D TiO_2 (c) and Kubelka–Munk plot for 2D TiO_2 (d).

method. The XRD pattern of the 2D TiO_2 sample is presented in Figure 1b. The signals corresponding to the primary reflections of TiO_2 can be observed at 25.3°, 36.9°, 37.7°, 38.5°, 48.0°, 53.8°, 55.0°, 62.2°, 62.6° and 70.2°. These signals can be associated with (101), (103), (004), (112), (200), (105) (211) (213) (204), and (220) anatase crystal planes (JCPDS card no. 21-1272). No other signals were observed, which confirmed the phase-pure anatase crystallographic structure of the obtained photocatalyst. The crystallite size calculated according to the Scherrer equation was about 24 nm, while $a = b$ and c crystal parameters were 3.768 and 9.517, respectively.

Furthermore, specific surface area and pore volume were analysed according to the BET method and the data are presented in Table 2. The fluffy, light powder of 2D TiO_2 exhibited a surface area of 12.9 $m^2 \cdot g^{-1}$ and a total pore volume of 0.0064 $cm^3 \cdot g^{-1}$.

The diffuse reflectance UV–vis spectrum of the prepared TiO_2 nanosheets is shown in Figure 1c. The TiO_2 photocatalyst exhibits strong absorption in the ultraviolet light wavelength range of 200–400 nm. As presented in Figure 1d, the optical bandgap (Eg) for TiO_2 calculated using the Tauc equation was about 3.18 eV. The 2D TiO_2 sample consisted of similar band gap energy compared to anatase, according to literature data with 3.2 eV (Khan et al., 2014).

The Mott–Schottky analysis was used to determine the location of E_{fb} by measuring the space charge region capacitance

Table 2. Summary of selected physical parameters of 2D TiO_2.

Sample label	Crystallite size [nm]	Crystal parameters [Å]			Surface area [$m^2 \cdot g^{-1}$]	Pore volume [$cm^3 \cdot g^{-1}$]	Bandgap E_g [eV]
		a	*b*	*c*			
2D TiO_2	24	3.786	3.786	9.517	12.9	0.0064	3.18

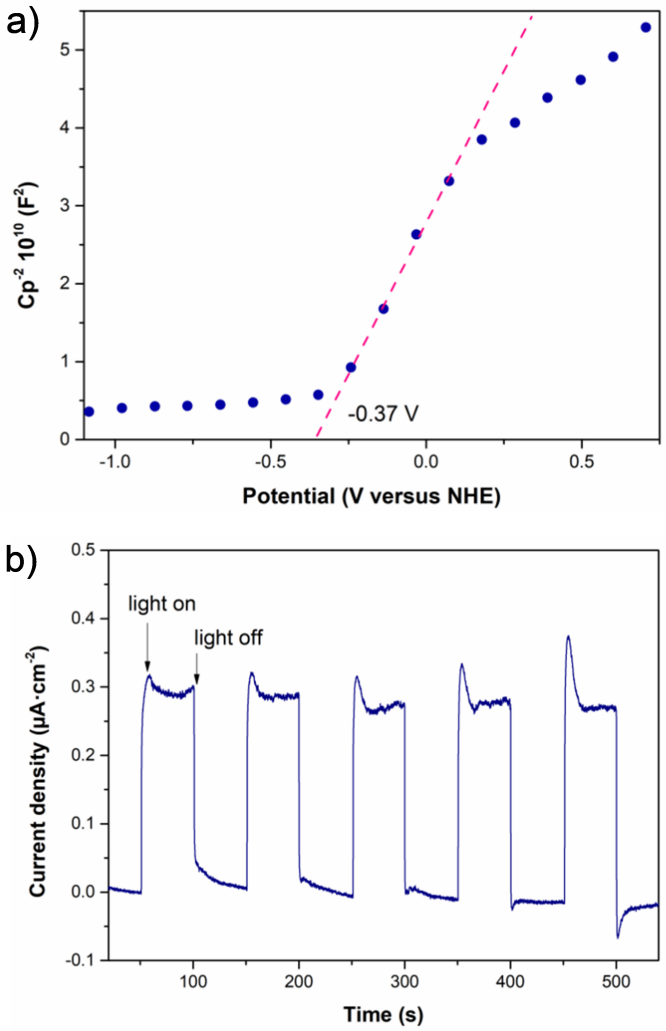

Figure 2. The Mott–Schottky plot for 2D TiO_2 (a), the transient photocurrent response curve of 2D TiO_2 (b).

(C_{sc}) at the electrode/electrolyte interface, see Figure 2a. The Mott–Schottky plots showed that TiO_2 acts as an n-type (negative slope) semiconductor. The flat band potential of 2D TiO_2 was estimated at –1.17 V vs Ag/AgCl and it is in good agreement with literature data (Sakai et al., 2004). For n-type semiconductors, the flat band potential is almost equal to the conduction band potential. Thus, according to values of E_{fb} and E_g, the valence band (VB) edge of 2D TiO_2 was determined at 2.01 V vs Ag/AgCl. Furthermore, the potential of 2D TiO_2 flat band edge position was converted to a value of –0.37 eV vs. NHE and the valence band edge location was estimated at 2.81 V vs. NHE. A positive location of VB can be associated with a high oxidation power. The photogenerated charge carrier separation and transfer rate were determined using photocurrent responses, shown in Figure 2b. The photocurrent increased when the light was switched on and decreased when the light was off, indicating that the photocatalyst respond to light with good reproducibility. Furthermore, photocurrent responses maintain stability after five on/off cycles implying the electrode was highly conductive and photoresponsive, and the photocatalyst may restrain photocorrosion.

3.2. Light-induced degradation of artificial sweeteners

The light-induced degradation of selected artificial sweeteners was studied using UV light (photolysis process), UV/PMS, UV/TiO_2/PMS, and UV/TiO_2/PMS systems. Results of the degradation efficiency within the irradiation time for acesulfame (ACE), aspartame (ASP), cyclamate (CYC) and saccharin (SACH) are presented in Figure 3. Before each photocatalytic process in the presence of 2D TiO_2, the sweetener aqueous solution containing photocatalyst was kept in the dark for 30 min under continuous stirring to achieve adsorption–desorption equilibrium. The adsorption ability was negligible (less than 3%), and this process is not considered to play an important role in the sweetener removal. Furthermore, artificial sweeteners as persistent organic compounds were not degraded by light in the direct photolysis process. Only SACH underwent the process of photolytic decomposition. However, the degradation efficiency was only 7% after 30 min and 10% after 60 min of irradiation. The enhanced degradation of artificial sweeteners was observed in UV/PMS system. After 30 min of irradiation, about 29% of ACE, 72% of ASP, 37% of CYC and 38% of SACH were degraded, respectively. Furthermore, the degradation of artificial sweeteners was markedly improved in the presence of 2D TiO_2, and the total photodegradation of the parent compound was achieved for ACE and CYC after 20 minutes of irradiation, while ASP and SACH degraded in 94% and 91% within 30 min of irradiation. In comparison, 2D TiO_2 nanosheets revealed higher saccharin photocatalytic degradation than commercial TiO_2 P25. For acesulfame degradation, commercial TiO_2 P25 exhibited higher degradation rate of about 0.327 min^{-1} compared to 2D TiO_2. However, TiO_2 P25 possessed 4 times larger surface area than TiO_2 nanosheets, and therefore the per surface activity of 2D TiO_2 was higher in artificial sweetener degradation than commercial TiO_2 P25.

Furthermore, the coupling system of UV/TiO_2/PMS resulted in the most efficient photodegradation of all examined persistent organic pollutants with their complete degradation after 10 minutes for ACE and CYC and 15 minutes for ASP and SACH.

The advanced oxidation processes fitted well to the first-order kinetic reaction ($R^2 > 97\%$), and the values of first-order kinetic rate constants are summarised in Table 3. Peroxymonosulfate-assisted photocatalytic degradation of artificial sweeteners is reflected by the high synergistic factor $S_{UV/TiO2/PMS}$ values. The enhancement of the UV/TiO_2/PMS system results from the generation of sulfate and hydroxyl radical as a consequence of PMS activation and the reaction of HSO_5^- with e^- on the surface of 2D TiO_2,

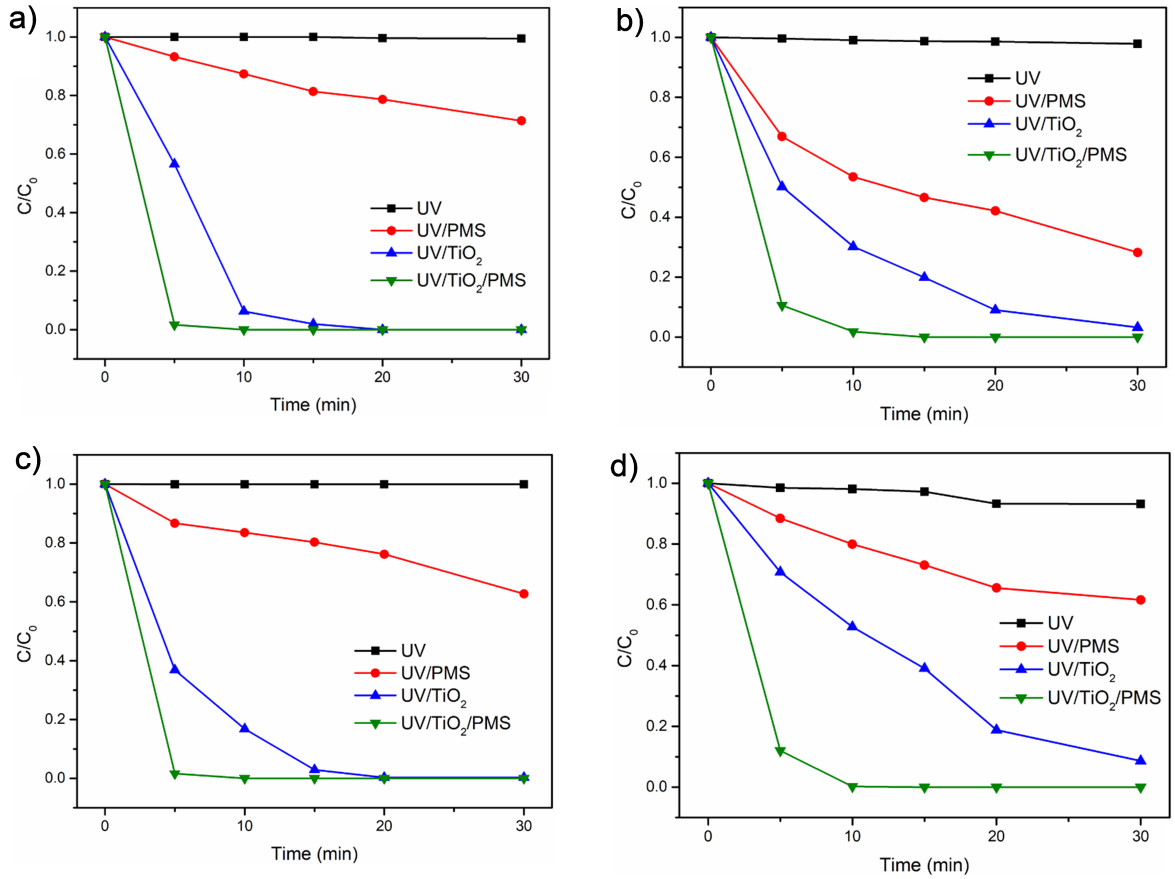

Figure 3. Light-induced degradation of acesulfame (a), aspartame (b), cyclamate (c) and saccharin (d).

leading to $SO_4^{\bullet -}$ and •OH production, according to Equations (1)–(2) (Rodríguez-Chueca et al., 2019).

$$HSO_5^- + e^- \rightarrow SO_4^{\bullet -} + HO^- \quad (1)$$

$$HSO_5^- + e^- \rightarrow SO_4^{2-} + HO^{\bullet} \quad (2)$$

Remarkably, the $S_{UV/TiO2/PMS}$ values depended on the degraded artificial sweetener and the highest synergistic factor was noticed for SACH photo-assisted degradation.

The mineralisation efficiency measured as total organic carbon (TOC) removal is another important parameter reflecting the progress in the degradation of organic pollutants. The degradation efficiency and TOC removal in the UV/PMS process of ACE, ASP, CYC were consistent, showing the lowest removal efficiency of organic pollutants. For SACH the TOC reduction was not observed. The highest effect of TOC reduction of about 91% was observed for UV/TiO_2 processes during the degradation of ACE and SACH. Furthermore, the mineralisation efficiency in the UV/TiO_2/PMS system of each artificial sweetener was about 70%.

A schematic illustration of the photocatalytic mechanism of artificial sweetener degradation in the presence of a PMS-assisted photodegradation process is proposed and presented in Figure 5. In the heterogeneous photocatalysis process, the reaction proceeds with the participation of photogenerated charge carriers. The photocatalytic properties of semiconductors are explained by their electronic structure. The ex-

Table 3. The efficiency of artificial sweeteners degradation by the UV/TiO_2, UV/PMS and UV/TiO_2/PMS advanced oxidation processes.

Sweetener	Type of process	First-order kinetic rate constant	Synergistic factor $S_{UV/TiO2/PMS}$
ACE	UV/PMS	0.0168	2.76
	UV/2D TiO_2	0.279	
	UV/2D TiO_2/PMS	0.818	
ASP	UV/PMS	0.0418	3.02
	UV/2D TiO_2	0.107	
	UV/2D TiO_2/PMS	0.449	
CYC	UV/PMS	0.0116	3.46
	UV/2D TiO_2	0.228	
	UV/2D TiO_2/PMS	0.829	
SACH	UV/PMS	0.0165	5.38
	UV/2D TiO_2	0.0622	
	UV/2D TiO_2/PMS	0.424	

citation of 2D TiO_2 occurs as a result of the absorption of light with energy equal to or greater than the bandgap energy ($\geq$ 390 nm). As a result of excitation, an electron is transferred from the valence band (VB) of TiO_2 to the conduction band (CB), generating excited electrons (e^-) and an unoccupied energy level named holes (h^+). The photogenerated electrons at the surface of 2D TiO_2 reduce dissolved molecular oxygen to superoxide anion radicals with strong oxidation ability (–0.33 V vs. NHE). Simultaneously, the photogenerated electrons can be trapped by adsorbed PMS to generate both $SO_4^{\bullet -}$ and $^{\bullet}OH$ radicals. In the presence of water molecules or hydroxide ions, the holes can generate hydroxyl

Table 4. The comparison of this work with results presented in recent related papers.

Advanced treatment process	Artificial sweetener	Light source	Time	Degradation efficiency [%]	References
H_2O_2	ACE	UV-LED $\lambda \sim 265$ nm	120 min	85	(Wang et al., 2019b)
TiO_2				90.4	
ZnO				62.7	
PMS				76.9	
PDS				85.56	
PMS + O_3	ACE	without light	15 min	90.4	(Shao et al., 2019)
O_3				52.7	
PMS				0	
·OH (radiolysis of water)	ACE	pulsed 8 MeV electron beam from the linear accelerator	μs	67.9	(Toth et al., 2012)
	ASP			52.2	
	SACH			52.7	
PDS	ACE	UV medium pressure mercury lamp ($\lambda \sim 365$ nm) (500 W)	6 min	100	(Xue et al., 2020)
photolysis	ACE	UV medium pressure mercury lamp (150 W)	30 min	0	in the present study
PMS			30 min	29	
2D TiO_2			15 min 20 min	98 100	
2D TiO_2+ PMS			5 min 10 min	98 100	
photolysis	ASP	UV medium pressure mercury lamp (150 W)	30 min	0	in the present study
PMS			30 min	72	
2D TiO_2			30 min	97	
2D TiO_2+ PMS			10 min 15 min	98 100	
photolysis	CYC	UV medium pressure mercury lamp (150 W)	30 min	0	in the present study
PMS			30 min	37	
2D TiO_2			15 min 20 min	97 100	
2D TiO_2+ PMS			5 min 10 min	98.5 100	
photolysis	SACH	UV medium pressure mercury lamp (150 W)	30 min	7	in the present study
PMS			30 min	38	
2D TiO_2			30 min	91	
2D TiO_2+ PMS			5 min 10 min	88 99.8	

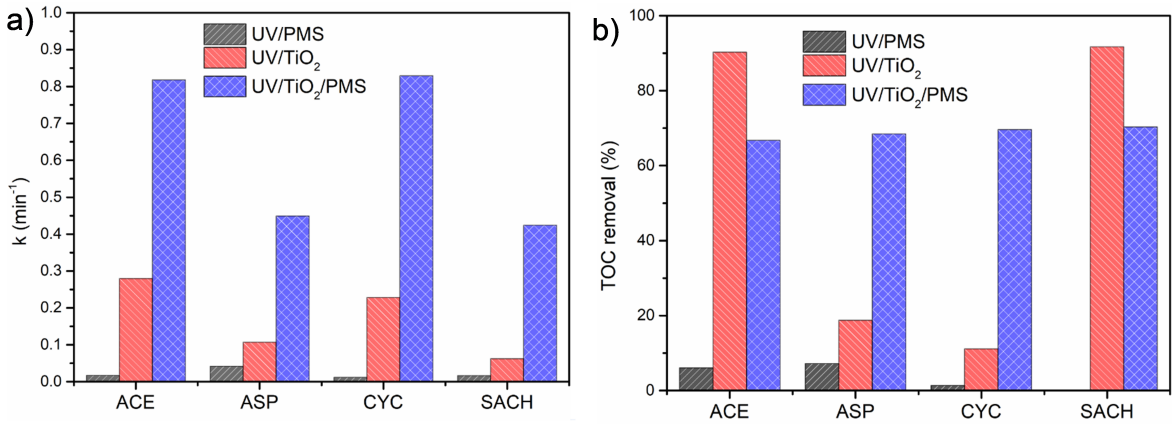

Figure 4. The summary of photolytic and photocatalytic degradation of ACE, ASP, CYC and SACH according to first-order kinetic rate constant (a) and TOC removal (b).

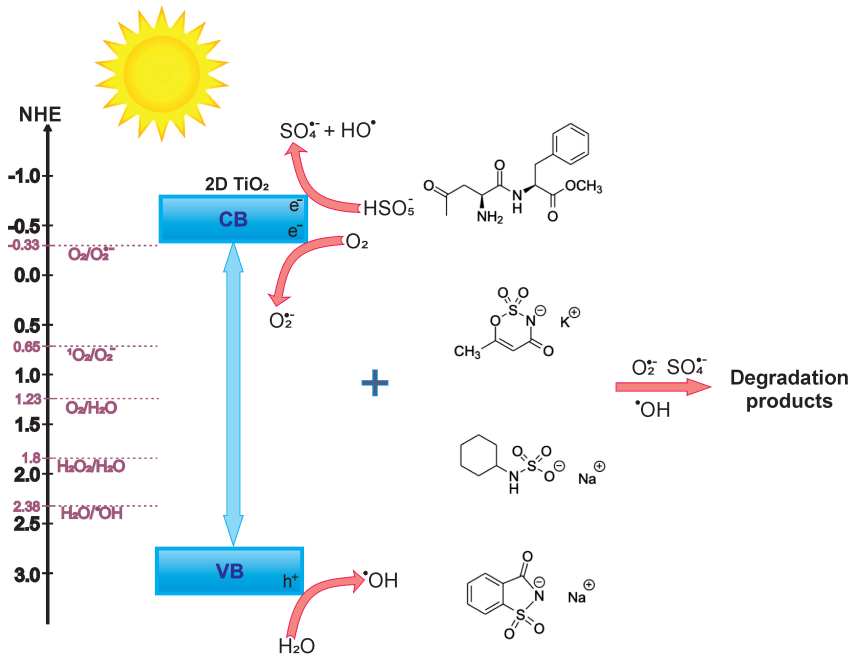

Figure 5. Proposed mechanism of PMS activation over TiO_2 nanosheets.

radicals. Furthermore, the photogenerated reactive species participate in the effective degradation and mineralisation of artificial sweeteners.

Finally, the photodegradation activity of UV/TiO_2/PMS system was compared with the previously reported advanced treatment processes used for the degradation of artificial sweeteners, and the results are shown in Table 4. It was found that the PMS-assisted photodegradation of artificial sweeteners over 2D TiO_2 in our work has excellent performance compared with other advanced treatment systems. For example, Wang et al. (2019b) studied the degradation of acesulfame under UV-LED controlled illumination. The highest degradation rate of acesulfame was observed for the UV-LED/TiO_2 system allowing for more than 90% of artificial sweetener degradation after 120 min of the photocatalytic process (Wang et al., 2019b). In our study, degradation of ACE was reached in 20 min of the photodegradation process in the presence of 2D TiO_2 and in only 10 min in the PMS-assisted photodegradation process. Shao et al. studied the degradation efficiency of ACE in the ozonation process combined with sulphate radicals produced from peroxymonosulfate (Shao et al., 2019). However, the ozonation and radiolysis of water reported by Toth et al. (2012) are restricted by the high operation costs and low mineralisation efficiency. In this regard, the photocatalysis process is an interesting intensification approach in AOPs, owing to the generation of electron-hole pairs under light irradiation and the production of reactive oxygen species. Furthermore, PMS acceleration properties allowed efficient degradation and mineralisation of artificial sweeteners in 5–30 min of the photodegradation process.

4. CONCLUSIONS

In the present study, the light-induced degradation of acesulfame, aspartame, cyclamate and saccharin was investigated with PMS-assisted process, photocatalysis and PMS-assisted photodegradation in the presence of TiO_2 nanosheets synthesised successfully via lyophilisation method. The degradation of artificial sweeteners followed pseudo-first-order kinetics. It was found that the studied artificial sweeteners were not susceptible to photolysis within 60 minutes of irradiation under UV light. Further, the PMS-assisted photodegradation process is a promising advanced oxidation method for the degradation of persistent organic pollutants not susceptible to biodegradation from wastewater due to its high performance resulting from efficient $SO_4^{\bullet-}$, $O_2^{\bullet-}$ and $^{\bullet}OH$ in-situ generation. In the presence of 2D titanium (IV) oxide, the artificial sweeteners were degraded entirely in less than 30 min, whereas the addition of 0.5 mM of peroxymonosulfate resulted in efficient degradation within less than 15 min of the advanced treatment process.

ACKNOWLEDGMENTS

The research was financially supported by the Gdańsk University of Technology within the RADIUM program (DEC-15/RADIUM/2022).

REFERENCES

Basson A.R., Rodriguez-Palacios A., Cominelli F., 2021. Artificial sweeteners: History and new concepts on inflammation. *Front. Nutr.*, 8, 746247. DOI: 10.3389/fnut.2021.746247.

Cong W., Wang R., Cai H., Daimon C. M., Scheibye-Knudsen M., Bohr V.A., Turkin R., Wood III W.H., Becker K.G., Moaddel R., Maudsley S., Martin B., 2013. Long-term artificial sweetener acesulfame potassium treatment alters neurometabolic functions in C57BL/6J mice. *PLoS ONE*, 8, e70257. DOI: 10.1371/journal.pone.0070257.

Erbaş O., Erdoğan M.A., Khalilnezhad A., Solmaz V., Gürkan F.T., Yiğittürk G., Eroglu H.A., Taskiran D., 2018. Evaluation of long-term effects of artificial sweeteners on rat brain: a biochemical, behavioral, and histological study. *J. Biochem. Mol. Toxicol.*, 32, e22053. DOI: 10.1002/jbt.22053.

Jia W., Ling Y., Lin Y., Chang J., Chu X., 2014. Analysis of additives in dairy products by liquid chromatography coupled to quadrupole-orbitrap mass spectrometry. *J. Chromatogr. A*, 1336, 67–75. DOI: 10.1016/j.chroma.2014.02.028.

Khan M.M., Ansari S.A., Pradhan D., Ansari M.O., Han D.H., Lee J., Cho M.H., 2014. Bandgap engineered TiO_2 nanoparticles for visible light induced photoelectrochemical and photocatalytic studies. *J. Mater. Chem. A.*, 2, 637–644. DOI: 10.1039/c3ta14052k.

Kokotou M.G., Asimakopoulos A.G., Thomaidis N.S., 2012. Artificial sweeteners as emerging pollutants in the environment: analytical methodologies and environmental impact. *Anal. Methods*, 4, 3057. DOI: 10.1039/c2ay05950a.

Malinowska I., Kubica P., Madajski P., Ostrowski A., Gómez Polo C., Carvera L., Bednarski W., Zielińska-Jurek A., 2023. Synthesis, characterisation, and application of 2D/2D TiO_2-GO-$ZnFe_2O_4$ obtained by the fluorine-free lyophilisation method for solar light-driven photocatalytic degradation of ibuprofen. *Environ. Sci. Pollut. Res.*, 30, 35929–35944. DOI: 10.1007/s11356-022-24587-0.

Naik A.Q., Zafar T., Shrivastava V.K., 2021. Environmental impact of the presence, distribution, and use of artificial sweeteners as emerging sources of pollution. *J. Environ. Public Health*, 2021, 6624569. DOI: 10.1155/2021/6624569.

Oser B.L., Carson S., Cox G.E., Vogin E.E., Sternberg S.S., 1975. Chronic toxicity study of cyclamate: Saccharin (10 :1) in rats. *Toxicology*, 4, 385–386. DOI: 10.1016/0300-483x(75)90054-2.

Perkola N., Vaalgamaa S., Jernberg J., Vähätalo A.V., 2016. Degradation of artificial sweeteners via direct and indirect photochemical reactions. *Environ. Sci. Pollut. Res.*, 23, 13288–13297. DOI: 10.1007/s11356-016-6489-4.

Praveena S.M., Cheema M.S., Guo H.-R., 2019. Non-nutritive artificial sweeteners as an emerging contaminant in environment: A global review and risks perspectives. *Ecotoxicol. Environ. Saf.*, 170, 699–707. DOI: 10.1016/j.ecoenv.2018.12.048.

Renwick A.G., Thompson J.P., O'Shaughnessy M., Walter E.J., 2004. The metabolism of cyclamate to cyclohexylamine in humans during long-term administration. *Toxicol. Appl. Pharmacol.*, 196, 367-80. DOI: 10.1016/j.taap.2004.01.013.

Rodríguez-Chueca J., Alonso E., Singh D.N., 2019. Photocatalytic mechanisms for peroxymonosulfate activation through the removal of methylene blue: A case study. *Int. J. Environ. Res. Public Health*, 16, 198. DOI: 10.3390/ijerph16020198.

Sakai N., Ebina Y., Takada K., Sasaki T., 2004. Electronic band structure of titania semiconductor nanosheets revealed by electrochemical and photoelectrochemical studies. *J. Am. Chem. Soc.*, 126, 5851–5858. DOI: 10.1021/ja0394582.

Sang Z., Jiang Y., Tsoi Y.-K., Leung K.S.-Y., 2014. Evaluating the environmental impact of artificial sweeteners: A study of their distributions, photodegradation and toxicities. *Water Res.*, 52, 260–274. DOI: 10.1016/j.watres.2013.11.002.

Shao Y., Pang Z., Wang L., Liu X., 2019. Efficient degradation of acesulfame by ozone/peroxymonosulfate advanced oxidation process. *Molecules,* 24, 2874. DOI: 10.3390/molecules24162874.

Toth J.E., Rickman K.A., Venter A.R., Kiddle J.J., Mezyk S.P., 2012. Reaction kinetics and efficiencies for the hydroxyl and sulfate radical based oxidation of artificial sweeteners in water. *J. Phys. Chem. A.*, 16, 9819–9824. DOI: 10.1021/jp3047246.

Wacławek S., Lutze H.V., Grübel K., Padil V.V.T., Černík M., Dionysiou D.D., 2017. Chemistry of persulfates in water and wastewater treatment: A review. *Chem. Eng. J.*, 330, 44–62. DOI: 10.1016/j.cej.2017.07.132.

Wang C., Kim J., Malgras V., Na J., Lin J., You J., Zhang M., Li J., Yamauchi Y., 2019a. Metal-organic frameworks and their derived materials: Emerging catalysts for a sulfate radicals-based advanced oxidation process in water purification. *Small*, 15, 1900744. DOI: 10.1002/smll.201900744.

Wang Z., Thuy G.N.S.T., Srivastava V., Ambat I., Sillanpää M., 2019b. Photocatalytic degradation of an artificial sweetener (Acesulfame-K) from synthetic wastewater under UV-LED controlled illumination. *Process Saf. Environ. Prot.*, 123, 206-214. DOI: 10.1016/j.psep.2019.01.018.

Xu Y., Lin Z., Wang Y., Zhang H., 2017. The UV/ peroxymonosulfate process for the mineralisation of artificial sweetener sucralose. *Chem. Eng. J.*, 317, 561–569. DOI: 10.1016/j.cej.2017.02.058.

Xue H., Gao S., Li M., Wang Y., Liu B., 2020. Performance of ultraviolet/persulfate process in degrading artificial sweetener acesulfame. *Environ. Res.*, 188, 109804. DOI: 10.1016/j.envres.2020.109804.

Yang J., Zhu M., Dionysiou D.D., 2021. What is the role of light in persulfate-based advanced oxidation for water treatment? *Water Res.*, 189, 116627. DOI: 10.1016/j.watres.2020.116627.

Zelinski D.W., dos Santos T.P.M., Takashina T.A., Leifeld V., Igarashi-Mafra L., 2018. Photocatalytic degradation of emerging contaminants: Artificial sweeteners. *Water Air Soil Pollut.*, 229, 207. DOI: 10.1007/s11270-018-3856-4.

Zhong M., Wang T., Zhao W., Huang J., Wang B., Blaney L., Bu Q., Yu G., 2022. Emerging organic contaminants in chinese surface water: Identification of priority pollutants. *Engineering*, 11, 111-125. DOI: 10.1016/j.eng.2020.12.023.